ELSEVIER

Experimental Hematology

Experimental Hematology 2008;36:1524–1534

Tumorigenic potential and disease manifestations of malignant B-cell variants differing in their fibronectin adhesiveness

Liat Nadav[a,d], Vyacheslav Kalchenko[b], Meir Max Barak[c], Elizabeth Naparstek[d,e], Benjamin Geiger[a], and Ben-Zion Katz[d,e]

[a]*Departments of Molecular Cell Biology;* [b]*Veterinary Resources;* [c]*Structural Biology, Weizmann Institute of Science, Rehovot, Israel;* [d]*Hematology Institute, Tel Aviv Sourasky Medical Center;* [e]*Sackler Faculty of Medicine, Tel Aviv University, Tel Aviv, Israel*

(Received 31 January 2008; revised 22 April 2008; accepted 19 May 2008)

Objective. **Microenvironmental interactions of malignant B cells can modulate various in vitro physiological responses, including proliferation, migration, apoptosis, and drug resistance. Disease manifestations of human malignant B-cell variants, isolated based on their differential interactions with fibronectin, were examined in nonobese diabetic/severe combined immunodeficient (NOD/SCID) mice.**

Materials and Methods. **Disease manifestations were assessed by pathological examinations and skeletal imaging of NOD/SCID mice injected with malignant B-cell variants. Dissemination patterns were analyzed by whole-body real-time imaging of mice injected with fluorescence-labeled malignant cells.**

Results. **Initial dissemination patterns and dynamics of both high (type A) and low (type F)-adherent variants, following intravenous inoculation, were similar. Both cell types reached the spleen and liver within 30 minutes after injection, then increasingly accumulated within the bone marrow. Mice injected with type-A cells developed multiple myeloma–like disease within the bone marrow, with multiple lytic bone lesions. In contrast, type-F cells displayed low tumorigenic capacity in spite of their efficient homing to the bone marrow niche. In addition, type-A cells grew as extramedullary tumors in some of the intravenous-inoculated mice, and formed solid tumors following subcutaneous injection. Both cell variants retained their characteristics surface markers following in vivo outgrowth as tumors, indicating that at least some of their properties are relatively stable.**

Conclusion. **Data suggest that the differential tumorigenicity of B-cell adhesive variants is attributable to the capacity of type-A cells to survive and proliferate within the bone marrow, rather than to different initial dissemination of the two cell populations.** © **2008 ISEH - Society for Hematology and Stem Cells. Published by Elsevier Inc.**

The B-cell lineage is the origin of various hematological malignancies, including acute and chronic leukemias, different types of aggressive and indolent lymphomas, and plasma cell dyscrasias (e.g., multiple myeloma). Various genetic events (e.g., chromosomal translocations) are involved in development of B-cell malignancies. Biochemical signals that govern generation of immunoglobulin diversity can also trigger molecular events involved in B-cell tumorigenesis [1,2]. Molecular lesions in B cells that can lead to malignancy development may also be initiated by viruses (e.g., Epstein-Barr virus [3,4]). Although cancer cells, in general, are considered less dependent on and/or responsive to regulatory factors and stimuli compared with their normal counterparts, many studies indicate that microenvironmental interactions play an important role in regulating malignant B-cell physiology [5]. For example, survival-promoting microenvironments can support growth of chronic lymphocytic leukemia (CLL) cells, and rescue them from cytotoxic therapy [6]. In the case of multiple myeloma (MM), the bone marrow (BM) stroma supplies growth factors and cytokines that are essential for growth of the malignant plasma cells and progression of the disease [7–9]. Moreover, adhesive interactions between MM cells and various constituents of the extracellular matrix are known to regulate key physiological activities of the malignant plasma cells, including proliferation and resistance to apoptosis and cytotoxic drugs [7,10–13].

Offprint requests to: Ben-Zion Katz, Ph.D., Hematology Institute, Tel Aviv Sourasky Medical Center, 6 Weizman Street, Tel Aviv 64239, Israel; E-mail: bkatz@tasmc.health.gov.il

0301-472X/08 $–see front matter.
doi: 10.1016/j.exphem.2008.05.009

A hallmark of tumorigenesis is genetic instability, resulting in generation of diverse populations of malignant cells [14]. In diffuse large B-cell lymphoma, the malignant cell population is diverse, and the extent of this diversity may correlate with high risk for disease relapse and resistance to therapy [15]. The possibility that microenvironmental factors generate diversity in B-cell malignancy in clinical specimens has been suggested previously, but the clinical significance of such variants has not yet been evaluated [16,17]. We previously demonstrated that the malignant B-cell line ARH-77 cell is heterogeneous in its matrix adhesiveness and migratory activity [16]. Using selective adsorption on fibronectin-coated surface, we isolated two subpopulations of ARH-77 B cells, one displaying highly adhesive/low motile properties (type A), and the other, low adhesive/highly motile phenotype (type F). The two subpopulations differ in several surface markers and display different cytoskeletal organization [16] as well as distinct gene expression profiles (Nadav et al., unpublished data). Moreover, variant subpopulations of MM cells have also been observed in patient samples, where cells expressing high levels of CD138 (similar to type-F cells) were found in the liquid phase of the BM, and low CD138 expressors (similar to type-A cells) were found firmly attached to the BM spicules [16]. In the present study, we analyzed the tumorigenic potential, in vivo dissemination patterns and disease manifestations of these two malignant B-cell populations. The findings indicate that while both cell types home similarly to the BM, the fibronectin-adhesive variant displays a much higher capacity to develop a malignant disease similar to human MM.

Materials and methods

Cells

The ARH-77, Epstein-Barr virus–transformed plasma cell line was kindly provided by Prof. Hanna Ben-Bassat (Hadassah Medical School, Jerusalem, Israel), and cultured as described previously [16]. Cells were subjected to serial adhesion cycles on fibronectin, yielding type-A and type-F cell populations as described previously [16].

Mice, irradiation, and inoculation

Nonobese diabetic/severe combined immunodeficient (NOD/SCID) mice, 4 to 6 weeks old, were obtained from Harlan laboratories Ltd. (Ein Kerem, Jerusalem) and maintained at the Veterinary resources facility of the Weizmann Institute of Science. All in vivo experiments were approved by the Weizmann Institute's Animal Care and Use Committee. Mice were exposed to 150 cGy (rads) radiation from a Gammacell 40 source. Twenty-four hours later, 1×10^7 cells of either type-A or type-F variants were injected into the tail veins of 20 female NOD/SCID mice, in two independent groups of 10. The mice were then observed daily until they developed apparent disease manifestations. For subcutaneous growth, 1×10^7 cells of either type-A or type-F variants were each injected into the flanks of five nonirradiated mice. These mice were also observed daily until they developed palpable tumors.

Cell adhesion assay

Cell adhesion assay was carried out as described previously [16]. Briefly, cells were plated for 30 minutes on 5-cm bacterial dishes coated with 15 μg/mL fibronectin (Sigma, St Louis, MO, USA). Dishes were then washed twice with phosphate-buffered saline (PBS) to remove nonattached cells and the remaining cells were counted microscopically.

Flow cytometry

Fluorescein isothiocyanate (FITC)–conjugated anti-CD138 and isotype-control IgG1 were purchased from DAKO (Glostrup, Denmark) and used according to manufacturer's instructions. For staining with directly labeled antibodies, 50-μL samples (5×10^5 cells) were incubated with 5 μL each of the designated monoclonal antibody at 4°C for 30 minutes and then washed with 2 mL PBS. From each sample, 3×10^4 events were acquired by FACSCalibur at a rate of 150 to 300 events per second, and analyzed using the CellQuest software (Becton Dickinson, San Jose, CA, USA).

Homing experiments in NOD/SCID mice

Homing of type-A and type-F cells was investigated using whole-body optical imaging. Groups of nine anesthetized mice were injected with type-A or type-F cells, labeled with near-infrared lipophilic carbocyanine dye [1,1′-dioctadecyl-3,3,3′,3′- tetramethylindotricarbocyanine iodide (DiR)] (Invitrogen, Carlsbad, CA, USA) [18]. Cells (1×10^7) were incubated in 10 mL PBS containing 3.5 μg/mL DiR dye, and 0.5% ethanol at 37°C for 30 minutes. Cells were then washed twice with PBS, and the viability of the labeled cells was verified by trypan blue staining. Labeled cells were then injected intravenously into NOD/SCID mice whose hair was removed previously. DiR has absorption and fluorescence maxima at 750 and 782 nm, respectively, which correspond to low-light absorption and autofluorescence in living tissues. This property enables harvesting of a significant signal from labeled cells, with very low tissue background levels [18]. Mice were then observed by an IVIS 100 Imaging System (Xenogen, Cranbury, NJ, USA). For higher magnification visualization of labeled cells in the skull, mice were scarified and the head skin was removed. An SZX12 microscope (Olympus, Tokyo, Japan) coupled with charged coupled device Pixelfly (PCO, Kelheim, Germany) and compatible filter set for DiR were used for observation.

Histopathology

Animals were sacrificed and tissues were excised and fixed in 10% phosphate-buffered formalin, embedded in paraffin, sectioned, and stained with hematoxylin eosin. Histopathological examination was performed with a Nikon E600 microscope (Nikon Corporation, Tokyo, Japan). Images were recorded with a Nikon DXM1200 camera (Nikon Corporation).

Micro–computed tomography

Mice were scanned with a GE Explore Locus Micro-CT System (GE Healthcare, Ontario, Canada). The three-dimensional images were analyzed using a Microview 3D Volume and Analysis Tool (GE Healthcare).

Results

Disease manifestations of adhesive B-cell variants in NOD/SCID mice

The main objective of the present study was to elucidate the tumorigenic properties of malignant B-cell variants that were isolated by differential adhesive interactions with fibronectin. The 1×10^7 highly adherent (type-A) or 1×10^7 poorly adherent (type-F) cells were injected into the tail veins of 20 NOD/SCID mice. Of the 20 mice injected with type-A cells, 11 developed tumors within 50 days (Fig. 1A), which were manifested in a variety of ways, depending on their location (Fig. 1B). Six of the 11 disease-bearing animals developed head swelling and a lateral tilt in their posture, compatible with a tumor originating in the skull, with the mass causing lateral pressure on the brain tissue (Fig. 1B). Two of the 11 disease-bearing animals developed hind-leg paralysis, due to spinal cord compression by the tumor (Fig. 1B). Three of them developed palpable tumors in the leg, in the cervical region, and in the scapula. The mean latency period prior to disease onset in mice injected with type-A cells was 40 days (Fig. 1A). In contrast, only 3 of 20 mice injected with type-F cells developed manifestations of disease: two of these displayed head swelling without lateral tilt, and one developed head swelling and hind-leg paralysis. Mean latency period in mice injected with type-F cells was 73 days (Fig. 1A). Similar results were obtained when lower numbers (2×10^6) of cells were injected (not shown). Parental ARH-77 cells exhibited intermediate level of tumorigenic activity (Fig. 1A). While intravenous injection enables cells to home into their normal physiological environment, subcutaneous inoculation is not considered orthotropic. Subcutaneous inoculations can therefore assess the ability of the cells to grow without physiological microenvironmental support or constraints. As shown in Figure 1A, four of five nonirradiated mice injected subcutaneously with type-A cells developed palpable tumors after a mean latency time of 35 days. None of the nonirradiated mice developed tumors following such injection with type-F cells.

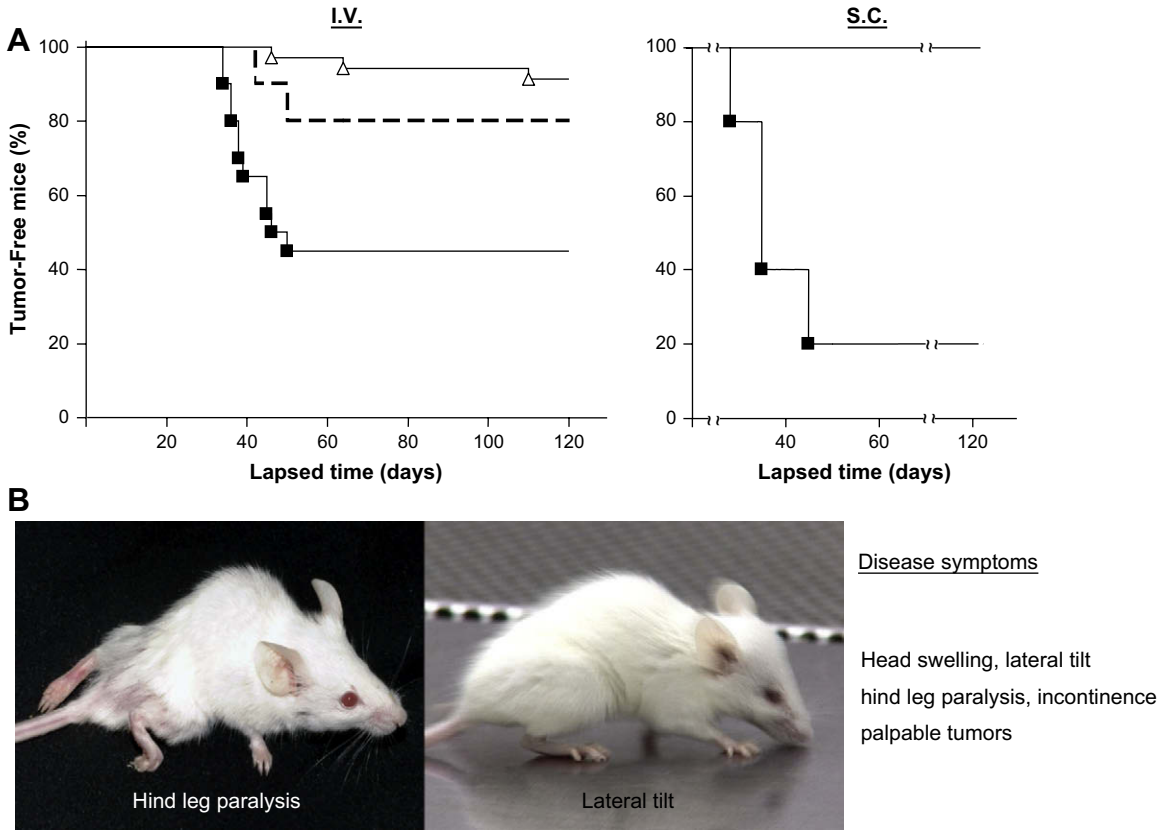

Figure 1. Disease incidence and clinical symptoms in nonobese diabetic/severe combined immunodeficient (NOD/SCID) mice, injected with type-A and type-F cell subpopulations.(**A**) Disease incidence and latency period seen in mice injected with type-A (closed colored squares) and type-F (open triangles) cells. Kaplan-Meier analysis of tumor onset shows a higher incidence of tumors in mice injected with type-A cells, as compared to those injected with type-F cells (mice injected intravenously: 11 of 20 as compared to 3 of 20; mice injected subcutaneously: 4 of 5 as compared to 0 of 5), and shorter latency period to disease onset in type-A injected mice. Also shown: Tumor incidence in mice injected with parental ARH-77 cells (dashed line). (**B**) Clinical manifestations in disease-bearing mice. Pictures show the most prevalent symptoms observed: hind-leg paralysis indicating a tumor in the thoracolumbar area of the spine, and lateral tilt in the posture accompanied by head swelling, indicating presence of a brain tumor. The few disease-bearing mice injected with type-F cells displayed the same symptoms (data not shown).

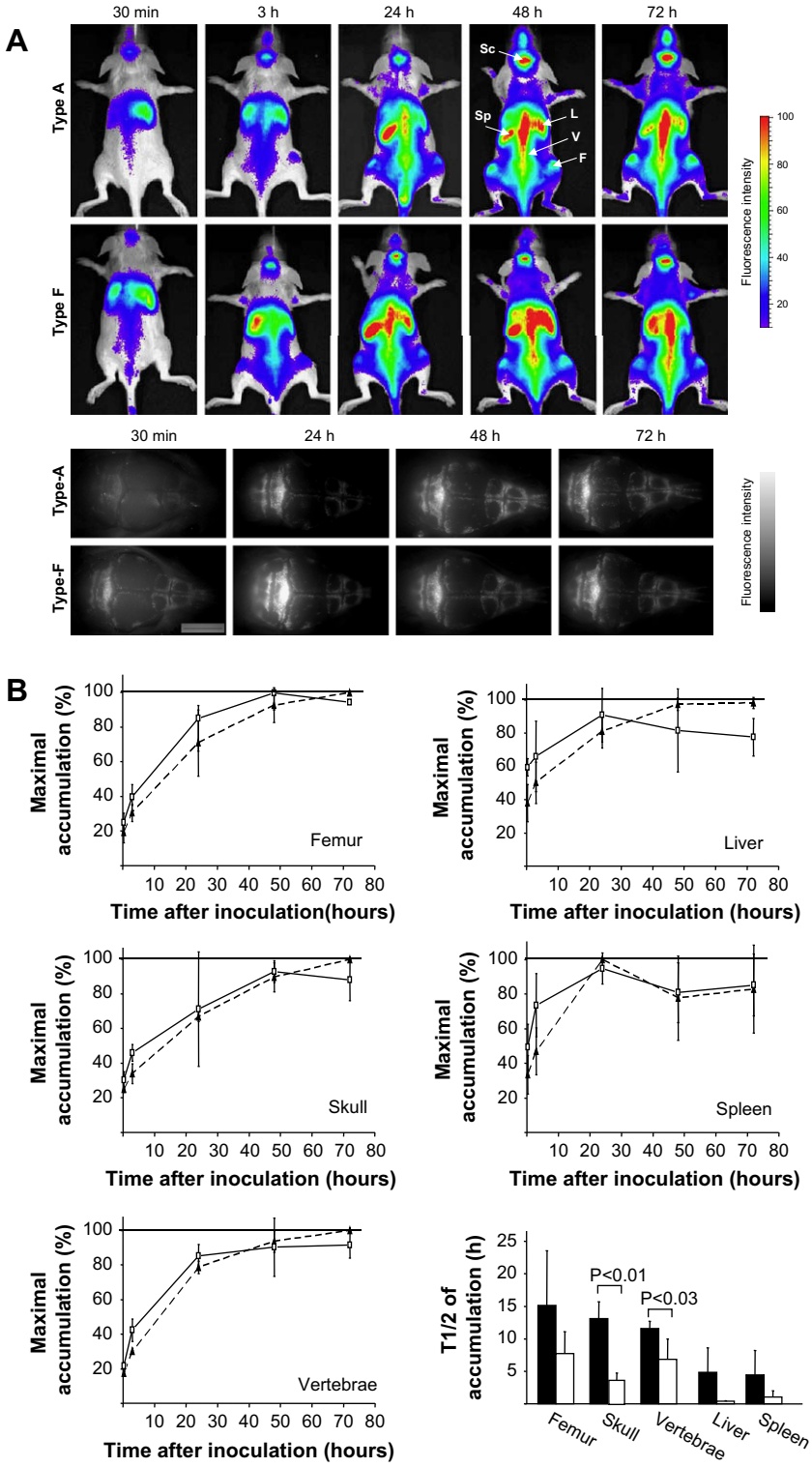

Figure 2. In vivo homing patterns and dynamics of type-A and type-F subpopulations in nonobese diabetic/severe combined immunodeficient (NOD/SCID) mice. (**A**) Noninvasive color-coded near-infrared fluorescent (NIRF) images of type-A and type-F homing in NOD/SCID mice. Upper panel: Images show massive primary homing to liver and spleen, and secondary homing to the bone marrow (BM). Type-A and type-F cells both home to the same organs. Images represent findings in at least three different mice. F = femur; L = Liver; Sk = Skull, Sp = Spleen, V = Vertebrae. Lower panel: high-resolution NIRF microscopic analysis of the cranium of a sacrificed NOD/SCID mouse after removal of skin, at different time points. The images show that the source of the cranium fluorescence is the BM, mainly in the area of the occipital sutures and not the brain tissue. Type-F cells accumulate in the skull more rapidly, reaching the maximal intensity after 24 hours, while signals from type-A cells reach the same intensity only after 72 hours. The cutoff of low-intensity light was adjusted to make a detected autofluorescent signal below the threshold. The monochrome-graduated bar and the color-graduated bar indicate

Dissemination patterns and dynamics of adhesive B-cell variants, as examined by whole-body optical imaging

A critical stage in the generation of hematopoietic malignancies involves the homing of the malignant cells to their physiologically relevant sites. We therefore examined in vivo the homing patterns and dynamics of the B-cell adhesive variants in the intravenous-inoculated mice, utilizing two complementary imaging tools: Whole-body optical imaging of the mice was performed at various time points following inoculation, followed by higher-resolution, microscopy-based imaging, which was utilized to observe the dissemination kinetics of the cells within the BM compartment in the skull. As shown in Figure 2, rapid accumulation of both type-A and type-F cells was observed in the spleen and liver, reaching $>50\%$ of the maximal value within 30 minutes, followed by significantly slower homing of cells into the BM of three independent organs, vertebrae, skull, and femur (Fig. 2A and B). The initial dynamics of the dissemination appeared to be somewhat faster for type-F cells, yet by 72 hours post inoculation the total accumulated fluorescence intensity was similar for both variants (Fig. 2A and B).

Fluorescence microscopy was further employed in order to track the dissemination of B-cell variants within the skull. As shown in Figure 2A (lower panel), distribution of the circulating cells was restricted to the BM of the skull, without penetrating into the brain tissue. These high-resolution images revealed cell aggregates in the BM, concentrating mainly in the fissures and occipital area, where the bone is relatively thick. Here again, type-F cells disseminated more rapidly than type-A cells, although 72 hours post inoculation, the overall fluorescence intensity of both variants was similar (Fig. 2A).

Analysis of osteolytic activity of adhesive B-cell variants in NOD/SCID mice, using micro–computed tomography

In order to characterize the disease manifestations in NOD/SCID mice, injected with type-A or type-F cells, treated and control mice were scanned by micro–computed tomography (micro-CT), which enables visualization of bone structure, density, and texture. Bone areas affected by tumors in several type-A injected mice displaying disease manifestations were visualized at higher resolution. Figure 3 (upper panel) depicts representative examples of several bony areas, including the hind leg, skull, lumbar, and cervical vertebrae of affected mice, as well as nonaffected mice, either injected with type-F cells, or untreated. The bone surface texture in mice injected with type-A cells was rough, affecting the fibula most severely (red arrow). Marked changes in the tibia texture were also observed, with a decline in mineralized bone structure. Bone mineral density (BMD) in the knee joint of this same mouse was compared to that of a normal-looking knee from a mouse injected with type-F cells (Fig. 3, lower panel) or untreated mouse (not shown). This analysis demonstrated areas of reduced BMD in the tibia of the mouse injected with type-A cells (red arrow), as well as foci, apparently representing lytic lesions (red arrowhead) where no minerals were detected. The skull of the mouse injected with type-A cells was also found to be severely affected (Fig. 3, top), sustaining damage that could have been caused by a combination of several distinct effects. Changes in the bone texture along both the outer and inner aspects of the skull (red arrow) reflect bone lysis. In addition, the fissures were open due to pressure caused by intracranial tumor growth from within the skull (red asterisk, and Fig. 5C). A BMD scan of the skull rim emphasized the lack of continuity, and the diminished BMD adjacent to the missing skull bone regions. In the lumbar vertebrae, the same elements of lytic lesions and altered bone texture were evident (red arrow); fractures in the cervical vertebrae were also seen (Fig. 3, red arrows).

Histopathological characteristics of disease generated by type-A cells

Mice injected with the highly adherent type-A cells developed MM-like disease, which disseminated throughout the body, leading to destruction of appendicular and long bones and nervous tissue, but with visceral sparing. Within bone and nervous tissues, multicentric disease was a regular finding. Typically, clinical manifestations only partially reflected the full extent of the lesions, as seen in postmortem examination. Figure 4A shows an example of massive neoplastic proliferation, which led to extensive destruction of the vertebral column and the loss of normal anatomic structures. Figure 4B depicts, at higher magnification, a view of a normal vertebra (black arrowhead) adjacent to a vertebra that has been largely obliterated by neoplastic infiltration (black arrow), with malignant cells extending beyond the vertebral body. These data indicate that although the proliferation of malignant cells may be initiated within the BM, their outgrowth is not necessarily confined to this compartment. In a similar manner, neoplastic growth was found in the subdural space of the skull, with destruction of calvaria (black arrow) (Fig. 4C); this tumor apparently originated from within the BM of the skull (Fig. 4D). In contrast,

fluorescence intensity in arbitrary units. (**B**) Kinetics of type-A and type-F cell homing in NOD/SCID mice (dashed line: type-A cells, solid line: type-F cells). Rate of cell accumulation in the liver and spleen is higher compared to that see in the BM, both for type-A and type-F cells. In the BM, the numbers of type-F cells reach a plateau after 48 hours and then tend to decrease, whereas the numbers of type-A cells continuously accumulate. Type-F cells accumulate more rapidly (significant results were obtained in the skull and vertebrae) within the different organs, as shown by lower T1/2 values (bar graph, bottom right) (white bars: type-F cells, black bars: type-A cells). Each point on the graph represents the average ± SD of three individual measurements performed on three different mice.

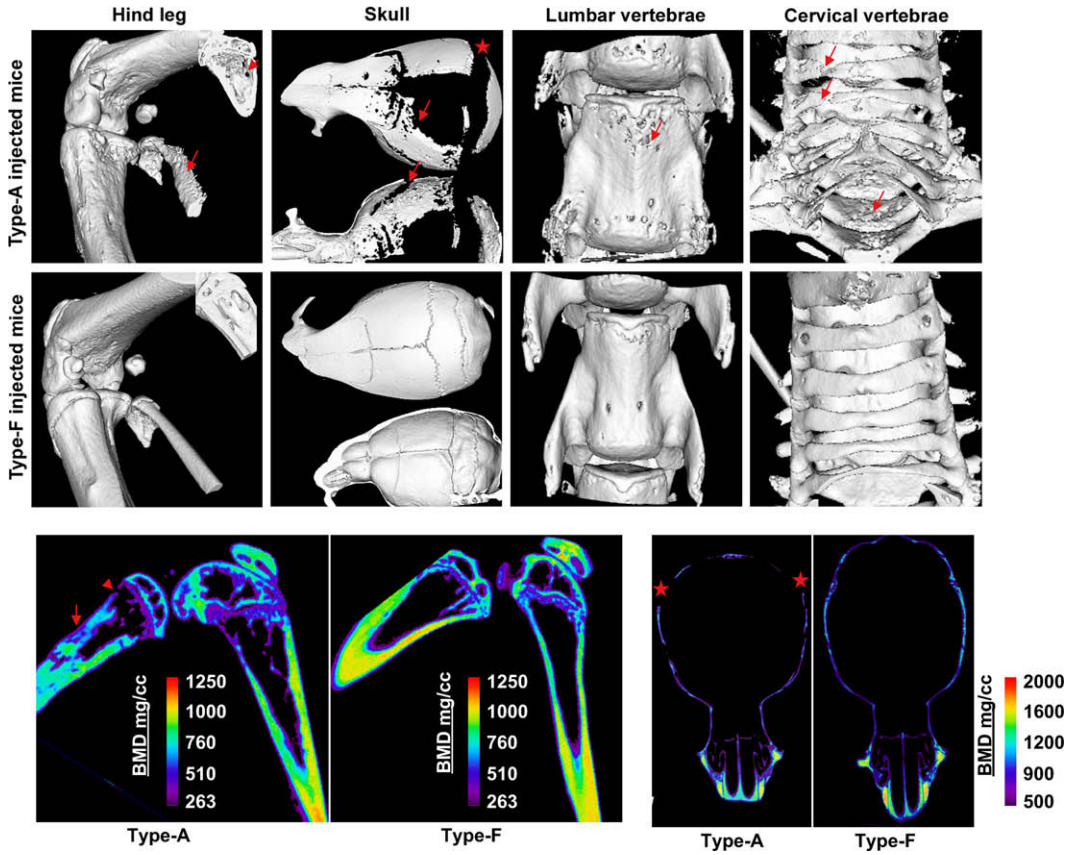

Figure 3. Micro-computed tomography skeleton imaging and bone mineral density (BMD) of mice injected with type-A and type-F cells. Upper panel: Images were taken from mice injected with type-A cells, in which disease manifestations and pathological findings were noted in the skull, the vertebral column and the leg. Images show altered bone texture in the fibula, skull, and vertebrae (red arrows), lytic lesions in the tibia (red arrowhead), detachment of the temporal and occipital bones in the area of the sutures due to pressure of the growing tumor from within the skull (red asterisks), and fractures in the cervical vertebrae (red arrow). Middle panel: Mice that were normal in appearance injected with type-F cells had no bone pathology. Lower panel: BMD decreased in areas of tumor and bone destruction, while adjacent areas are not affected. Two examples are the tibia, with areas of decreased BMD (red arrow), and areas with no bone detection at all (red arrowhead), that could represent lytic lesion. The femur in the diseased mouse resembles that of an unaffected control. In the skull of the diseased mouse, the surface of the cranium is not continuous (asterisks), and the existing bone manifests lower BMD.

the tumors seen in mice injected with type-F cells were usually solitary intracranial masses. One type-F mouse developed a combination of intracranial and vertebral masses.

In mice inoculated with type-A cells, the disease was manifested in neurological symptoms (e.g., head swelling, hind-leg paralysis). Pathological examination of tissue sections taken from these mice revealed considerable damage to nerve tissues. Figure 5A shows pronounced compression of the spinal cord (black arrow) as a result of neoplastic proliferation within the vertebral canal. Figure 5B indicates neoplastic infiltration (black arrowhead) of a dorsal root ganglion (black arrow). In our animal model, the disease produced nervous deficits associated with intracranial masses, causing mass effect and pressure on the brain. Figure 5C depicts one such example, an intracranial tumor (black arrow) pressing on and distorting the midbrain. Lateralization of the tumor clinically correlated with the head tilt that this mouse developed (Fig. 5, inset). High-resolution microscopic examination of the brain tissue (Fig. 5D) showed a discrete border between the tumor and the brain (marked with black arrowheads).

Ex vivo properties of tumor-derived type-A cells

Several tumors that grew in mice injected with type-A cells were explanted and grown in vitro in order to compare the tumor cells phenotype to that of the injected cell population. Adhesion assays demonstrated that cells derived from these tumors retained their highly adhesive phenotype regardless of the tumor site in vivo (Fig. 6A). In contrast, cells originating from the brain tumor isolated from mice injected with type-F cells did not adhere at all (data not shown), indicating that differences in adhesive properties between these two malignant plasma cell variants are retained in the developing tumor. Moreover, these results indicated that formation of tumors, albeit in rare cases, by type-F cells is not attributable to interconversion of type-F cells into type-A. We previously demonstrated that type-A and type-F cells differ in their flow cytometric profiles, including in expression of known MM-related antigens, such as CD138 [16]. As shown in Figure 6B, flow cytometric analysis of the cells originating from these tumors also conserved their flow cytometric profile. Thus, type-A cells, grown ex vivo, had lower levels of

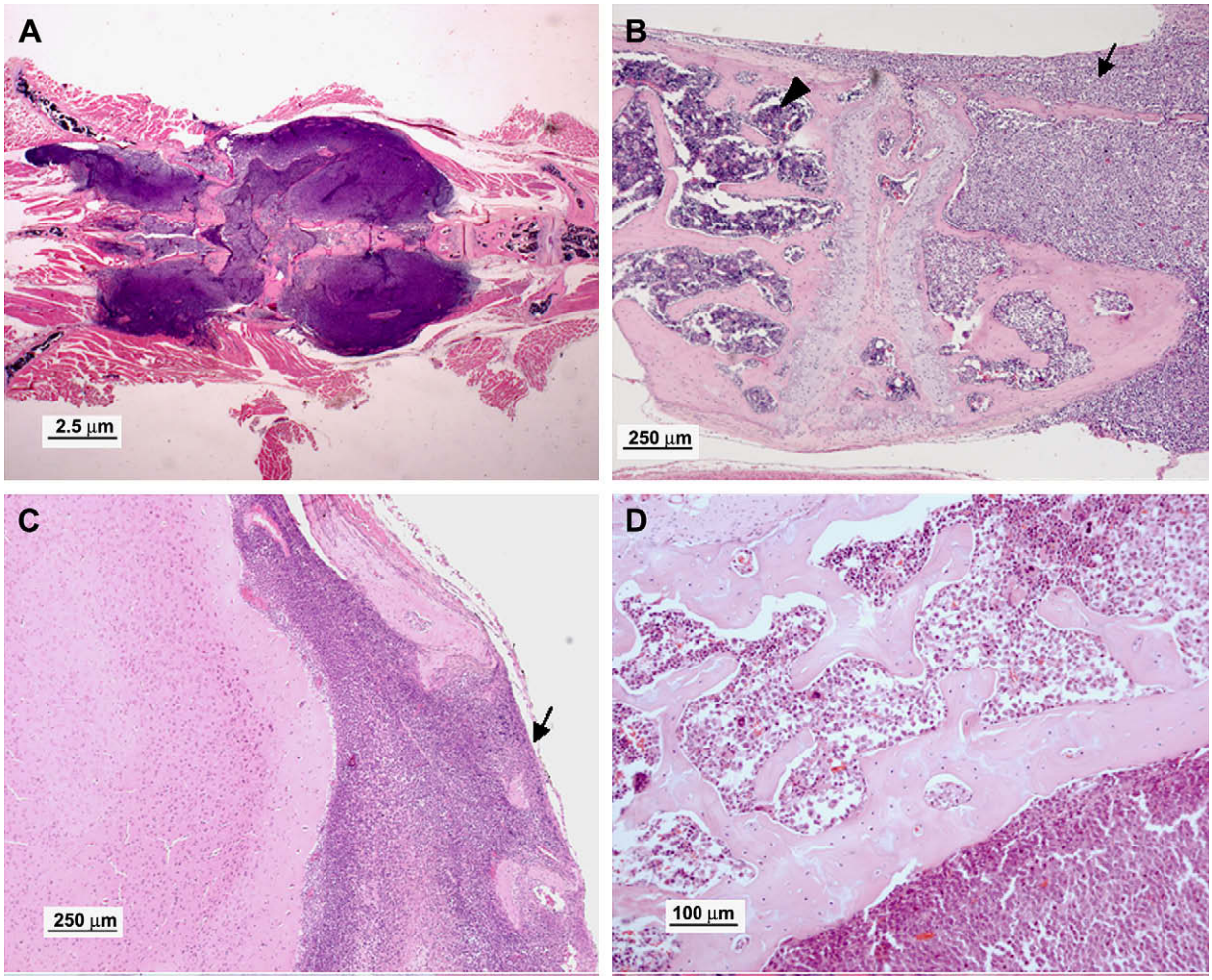

Figure 4. Destructive effects of growing multiple myeloma (MM) tumors on tissue. (**A**) Massive neoplastic proliferation leading to extensive destruction of the vertebral column and of normal anatomic structures. (**B**) View at high magnification of a normal vertebra (arrowhead) adjacent to a vertebra that has been largely obliterated by neoplastic infiltration (arrow). (**C**) Neoplastic growth in the subdural space of the skull with destruction of calvaria (arrow). (**D**) View at high magnification showing a tumor originating from the bone marrow (BM) of the skull bone.

CD138 compared to type-F cells: in fact, these levels were even lower than those of the cultured type-A cells, prior to inoculation. Similarly, cells originating from a brain tumor found in a mouse injected with type-F cells were characterized by CD138 expression levels that were even higher than those of the type-F cells originally injected into the mice (data not shown).

Discussion

Various studies indicate that extracellular matrix components of the BM microenvironment may play a crucial role in the pathogenesis of B-cell malignancies. Thus, adhesion to fibronectin via $\alpha_4\beta_1$ and $\alpha_5\beta_1$ integrins confers resistance to Fas-mediated apoptosis to neoplastic plasma cells, and interactions of MM cells with both free and immobilized vitronectin and fibronectin stimulate their proliferation [11,19]. In B-CLL, adhesion to fibronectin can induce transendothelial migration and invasion of the leukemic cells [20], or protect B-CLL cells from the cytotoxic effects of fludarabine [21]. These findings, demonstrating the capacity of matrix adhesion to affect the behavior and fate of cancer cells, compelled us to isolate adhesion variants from a B-cell malignancy and compare their properties [16]. In the present study, we directly examined whether adhesion variants of malignant B cells represent different tumorigenic potential in vivo, using the NOD/SCID mouse model, which was previously utilized to assess the malignancy of ARH-77 cells [22]. This assay indicated a significantly higher incidence of MM-like disease with a much shorter latency period in mice injected with the adhesive type-A B cells as compared to mice injected with the poorly adhesive type-F B cells.

Different tumorigenic properties of type-A and type-F cells could, in principle be attributed to a variety of cellular features, including cell homing into the BM, long-term

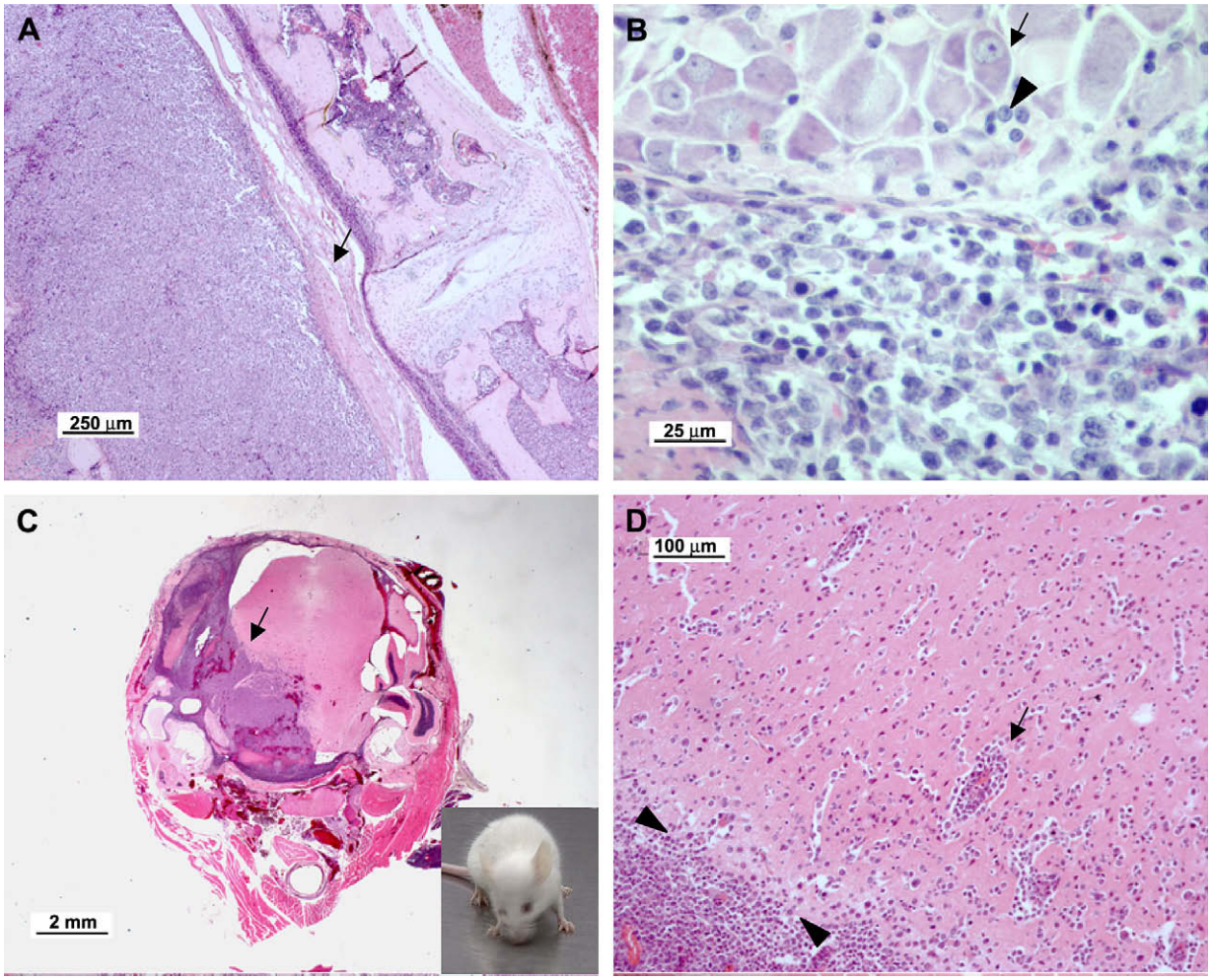

Figure 5. Damage to the nervous system inflicted by tumor growth. (**A**) Pronounced compression of the spinal cord (arrow) arising from neoplastic proliferation within the vertebral canal. (**B**) View at high magnification of neoplastic infiltration (arrow) of a dorsal root ganglion (arrowhead). (**C**) Tumor (arrow) presses and distorts the midbrain. Lateralization of the tumor clinically manifested itself as a head tilt (insert). (**D**) Malignant cells have low affinity to the neuroparenchyma. A discrete border is present between the tumor and the brain (marked by double arrowheads). The cortex is infiltrated by a low number of malignant cells that are mostly confined to the perivascular spaces of Virchow-Robbins (arrow).

survival in the BM niche, and capacity to proliferate in that site [23–26]. Specific homing of malignant cells to the target tissue is often considered critical for successful establishment and growth of tumors [26]. In order to determine whether the preferential development of disease by type-A cells is attributable to the higher capacity of these cells to reach the BM, we performed a short-term (up to 72 hours) homing analysis of the two variants. We found that the homing patterns of type-A and type-F cells were generally similar. Both variants disseminated mainly to the spleen, liver, and BM, which are the primary organs for MM cells [27]. It is nevertheless noteworthy that disease manifestations were detected only in the BM, without apparent involvement of the liver and spleen.

Although the general dissemination patterns of the two adhesive variants were similar, the homing of type-F cells was maximal at 24 hours, while type-A cells reached similar dissemination only after 72 hours. Supportive data obtained in our previous work [16] indicated that in vitro type-F cells migrate considerably faster than type-A cells. These data suggest that the low tumorigenic capacity of type-F cells is not attributable to poor BM homing, but rather to their poor long-term survival in the BM, and to the capacity to proliferate in that site. Collectively, our results indicate that establishment and development of disease is predominantly determined by interactions of the cells with the microenvironment in the target organs, rather then by restricted dissemination routes.

Micro-CT analysis provided striking information on the similarity between the disease model in mice, inoculated with type-A cells and human MM disease. Clear lines of similarity were noted, including major bone lesions, altered bone surface texture, fractures and, in some cases, complete loss of bone. We systematically measured BMD of the leg, thoracic

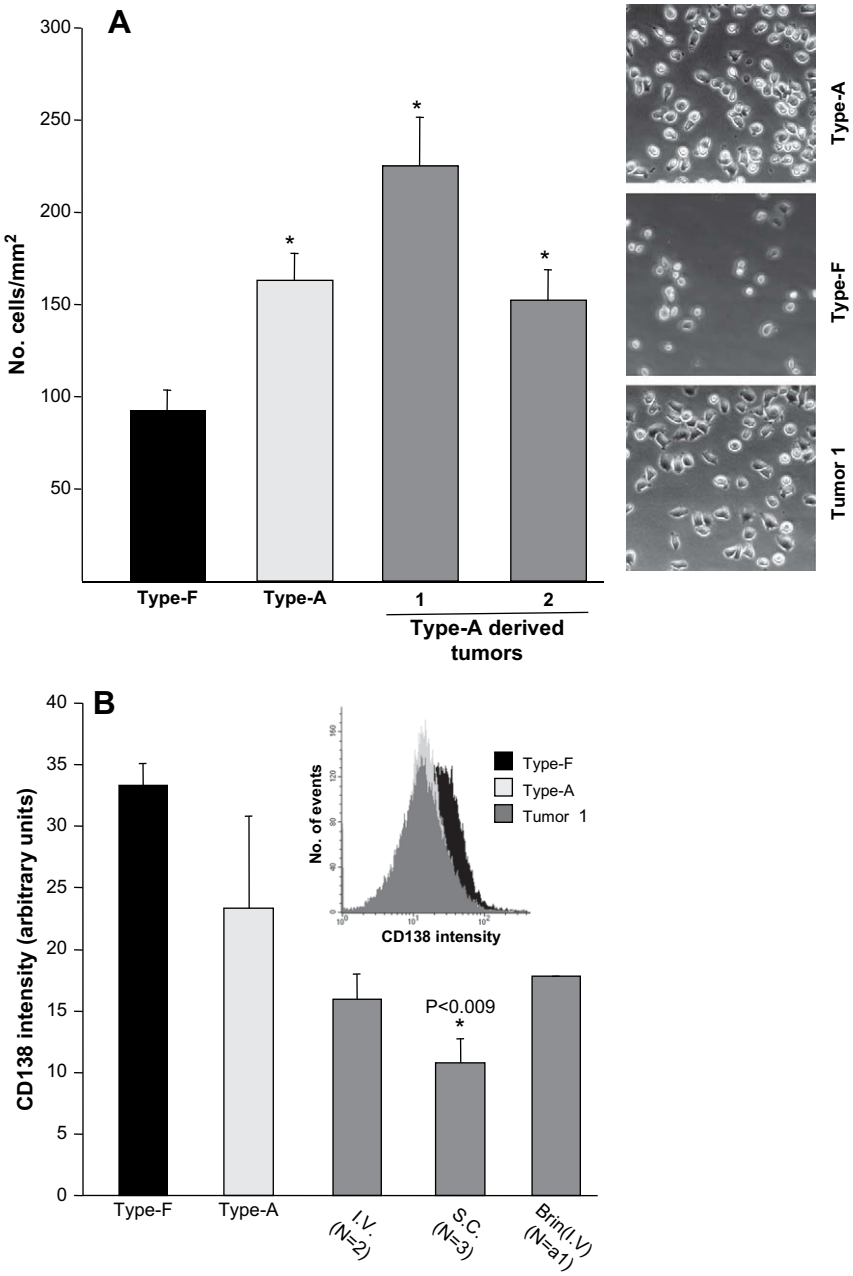

Figure 6. Cells isolated from mice injected with type-A cells retained their adhesive and flow-cytometry phenotype. (**A**) Tumors isolated from mice injected with type-A cells retained their adhesive phenotype, as demonstrated by an adhesion assay. Type-F cells (black bar) demonstrated low levels of adhesion, while type-A cells (white bar) and two tumors derived from mice injected with type-A cells (dark gray bars) were found to be highly adhesive (*$p < 0.05$, compared with type-F cells). One brain tumor isolated from a mouse injected with type-F cells showed a tendency to adhere that was even lower than that of the original type-F cells (data not shown). (**B**) CD138 expression levels are low in type-A cells (white bar) compared to those seen in type-F cells (black bar). This phenomenon was also observed in tumors derived from mice injected with type-A cells (light gray bars), whether intravenously or subcutaneously (even lower then type-A cells, * $p < 0.009$) injection. The insert shows a representative analysis of a tumor isolated after intravenous injection. The bars indicate an average ± standard deviation of tumors isolated after intravenous or subcutaneous injection, as well as one brain tumor.

vertebrae, and the skull, and found that low BMD is confined to areas where tumor growth was apparent. Previous studies with this technique have shown that BMD of the lumbar spine is often diminished in MM patients at diagnosis, whereas BMD of the hip is rarely affected, a finding that also corroborates the local effect suggested by our data [28,29].

An intriguing question highlighted by the present study is the possible causal relationships between the adhesive phenotype and the apparent tumorigenic properties. Two general mechanisms should be considered, namely, a direct involvement of matrix adhesion in the fine homing of malignant B cells into a specific BM niche, affecting their invasive growth

characteristics; or an indirect mechanism, whereby type-A cells exhibit higher survival capacity than type-F cells (related to, or independent of, integrin signaling). It is noteworthy that the increased tumorigenicity of type-A cells (compared to type-F) cannot be attributed to differences in the initial homing to BM, which was similar in the two adhesive variants. It should be mentioned that previous studies support the notion that highly adhesive cells have a growth advantage, which is enhanced by the cells' adhesion to the BM niche [30]. It was also found that cells with a highly adhesive phenotype characterize overt MM cells compared with the less adhesive plasma cells derived from smoldering myeloma patients [31]. Regulation of malignancy by other extracellular matrix proteins (e.g., thrombospondin-1) [32] and malignant clonal dominance by growth conditions [33] have already been established. Such studies clearly advocate for epigenetic regulatory modes of malignancy by microenvironmental factors and conditions.

Future studies may clarify the biochemical and molecular characteristics of adhesive malignant B cells (and MM cells in particular), thereby generating novel therapeutic targets. In this respect, it is already known that anti-adhesion therapy can significantly inhibit progression of MM and its clinical manifestations in murine models [34]. Moreover, anti-integrin–based agents may be utilized to overcome adhesion-mediated drug resistance [35]. Development of novel therapies for treatment of B-cell malignancies will be based on a deeper understanding of the basic molecular mechanisms driving this diversity.

Acknowledgments

This study was supported by grants from the Israel Science Foundation and the National Institute of General Medical Sciences grant for the Cell Migration Consortium (National Institutes of Health grant U54GM64346). B.G. holds the Erwin Neter Professorial Chair in Cell and Tumor Biology.

References

1. Ramiro AR, Nussenzweig MC, Nussenzweig A. Switching on chromosomal translocations. Cancer Res. 2006;66:7837–7839.
2. Gonzalez D, van der Burg M, Garcia-Sanz R, et al. Immunoglobulin gene rearrangements and the pathogenesis of multiple myeloma. Blood. 2007;110:3112–3121.
3. Epeldegui M, Widney DP, Martinez-Maza O. Pathogenesis of AIDS lymphoma: role of oncogenic viruses and B cell activation-associated molecular lesions. Curr Opin Oncol. 2006;18:444–448.
4. Young LS, Rickinson AB. Epstein-Barr virus: 40 years on. Nat Rev Cancer. 2004;4:757–768.
5. Kuppers R. Mechanisms of B-cell lymphoma pathogenesis. Nat Rev Cancer. 2005;5:251–262.
6. Munk Pedersen I, Reed J. Microenvironmental interactions and survival of CLL. B-cells. Leuk Lymphoma. 2004;45:2365–2372.
7. Mitsiades CS, Mitsiades NS, Munshi NC, Richardson PG, Anderson KC. The role of the bone microenvironment in the pathophysiology and therapeutic management of multiple myeloma: interplay of growth factors, their receptors and stromal interactions. Eur J Cancer. 2006;42:1564–1573.
8. Pagnucco G, Cardinale G, Gervasi F. Targeting multiple myeloma cells and their bone marrow microenvironment. Ann N Y Acad Sci. 2004;1028:390–399.
9. Roccaro AM, Hideshima T, Raje N, et al. Bortezomib mediates antiangiogenesis in multiple myeloma via direct and indirect effects on endothelial cells. Cancer Res. 2006;66:184–191.
10. Ng MH. Death associated protein kinase: from regulation of apoptosis to tumor suppressive functions and B cell malignancies. Apoptosis. 2002;7:261–270.
11. Ria R, Vacca A, Ribatti D, Di Raimondo F, Merchionne F, Dammacco F. Alpha(v)beta(3) integrin engagement enhances cell invasiveness in human multiple myeloma. Haematologica. 2002;87:836–845.
12. Garcia-Gila M, Lopez-Martin EM, Garcia-Pardo A. Adhesion to fibronectin via alpha4 integrin (CD49d) protects B cells from apoptosis induced by serum deprivation but not via IgM or Fas/Apo-1 receptors. Clin Exp Immunol. 2002;127:455–462.
13. Hazlehurst LA, Dalton WS. Mechanisms associated with cell adhesion mediated drug resistance (CAM-DR) in hematopoietic malignancies. Cancer Metastasis Rev. 2001;20:43–50.
14. Lengauer C, Kinzler KW, Vogelstein B. Genetic instabilities in human cancers. Nature. 1998;396:643–649.
15. Yang MH, Yen CC, Chiang SC, et al. Prognostic significance of clonal diversity of immunoglobulin gene rearrangements in patients with diffuse large B-cell lymphoma. Oncol Rep. 2005;13:503–508.
16. Nadav L, Katz BZ, Baron S, Cohen N, Naparstek E, Geiger B. The generation and regulation of functional diversity of malignant plasma cells. Cancer Res. 2006;66:8608–8616.
17. Zhu D, Orchard J, Oscier DG, Wright DH, Stevenson FK. V(H) gene analysis of splenic marginal zone lymphomas reveals diversity in mutational status and initiation of somatic mutation in vivo. Blood. 2002;100:2659–2661.
18. Kalchenko V, Shivtiel S, Malina V, et al. Use of lipophilic near-infrared dye in whole-body optical imaging of hematopoietic cell homing. J Biomed Opt. 2006;11: 050507.
19. Damiano JS, Cress AE, Hazlehurst LA, Shtil AA, Dalton WS. Cell adhesion mediated drug resistance (CAM-DR): role of integrins and resistance to apoptosis in human myeloma cell lines. Blood. 1999;93: 1658–1667.
20. Redondo-Munoz J, Escobar-Diaz E, Samaniego R, Terol MJ, Garcia-Marco JA, Garcia-Pardo A. MMP-9 in B-cell chronic lymphocytic leukemia is up-regulated by alpha4beta1 integrin or CXCR4 engagement via distinct signaling pathways, localizes to podosomes, and is involved in cell invasion and migration. Blood. 2006;108:3143–3151.
21. de la Fuente MT, Casanova B, Moyano JV, et al. Engagement of alpha4beta1 integrin by fibronectin induces in vitro resistance of B chronic lymphocytic leukemia cells to fludarabine. J Leukoc Biol. 2002;71:495–502.
22. Huang YW, Richardson JA, Tong AW, Zhang BQ, Stone MJ, Vitetta ES. Disseminated growth of a human multiple myeloma cell line in mice with severe combined immunodeficiency disease. Cancer Res. 1993;53:1392–1396.
23. Corre J, Mahtouk K, Attal M, et al. Bone marrow mesenchymal stem cells are abnormal in multiple myeloma. Leukemia. 2007;21: 1079–1088.
24. Perez LE, Parquet N, Shain K, et al. Bone marrow stroma confers resistance to Apo2 ligand/TRAIL in multiple myeloma in part by regulating c-FLIP. J Immunol. 2008;180:1545–1555.
25. Hecht M, von Metzler I, Sack K, Kaiser M, Sezer O. Interactions of myeloma cells with osteoclasts promote tumour expansion and bone degradation through activation of a complex signalling network and upregulation of cathepsin K, matrix metalloproteinases (MMPs) and urokinase plasminogen activator (uPA). Exp Cell Res. 2008;314: 1082–1092.

26. Vande Broek I, Vanderkerken K, Van Camp B, Van Riet I. Extravasation and homing mechanisms in multiple myeloma. Clin Exp Metastasis. 2008;25:325–334.
27. Vanderkerken K, De Greef C, Asosingh K, et al. Selective initial in vivo homing pattern of 5T2 multiple myeloma cells in the C57BL/KalwRij mouse. Br J Cancer. 2000;82:953–959.
28. Dhodapkar MV, Weinstein R, Tricot G, et al. Biologic and therapeutic determinants of bone mineral density in multiple myeloma. Leuk Lymphoma. 1998;32:121–127.
29. Abildgaard N, Brixen K, Eriksen EF, Kristensen JE, Nielsen JL, Heickendorff L. Sequential analysis of biochemical markers of bone resorption and bone densitometry in multiple myeloma. Haematologica. 2004;89:567–577.
30. Teoh G, Anderson KC. Interaction of tumor and host cells with adhesion and extracellular matrix molecules in the development of multiple myeloma. Hematol Oncol Clin North Am. 1997;11:27–42.
31. Silvestris F, Cafforio P, Calvani N, De Matteo M, Lombardi L, Dammacco F. In-vitro functional phenotypes of plasma cell lines from patients with multiple myeloma. Leuk Lymphoma. 2006;47:1921–1931.
32. Weinstat-Saslow DL, Zabrenetzky VS, VanHoutte K, Frazier WA, Roberts DD, Steeg PS. Transfection of thrombospondin 1 complementary DNA into a human breast carcinoma cell line reduces primary tumor growth, metastatic potential, and angiogenesis. Cancer Res. 1994;54:6504–6511.
33. Rak JW, Kerbel RS. Growth advantage ("clonal dominance") of metastatically competent tumor cell variants expressed under selective two- or three-dimensional tissue culture conditions. In Vitro Cell Dev Biol Anim. 1993;29A:742–748.
34. Mori Y, Shimizu N, Dallas M, et al. Anti-alpha4 integrin antibody suppresses the development of multiple myeloma and associated osteoclastic osteolysis. Blood. 2004;104:2149–2154.
35. Damiano JS. Integrins as novel drug targets for overcoming innate drug resistance. Curr Cancer Drug Targets. 2002;2:37–43.